

Transfer of photothermal nanoparticles using stem cell derived small extracellular vesicles for *in vivo* treatment of primary and multinodular tumors

Authors

María Sancho-Albero^{1,2,3,+}, Miguel Encinas-Gimenez^{1,2,3}, Victor Sebastián^{1,2,3}, Estela Pérez⁴, Lluís Luján^{4,5}, Jesús Santamaría^{1,2,3}, Pilar Martín-Duque^{6,7,#*}.*

¹Instituto de Nanociencia y Materiales de Aragón (INMA), CSIC-Universidad de Zaragoza, Zaragoza, Spain.

²Department of Chemical Engineering and Environmental Technologies, University of Zaragoza, Zaragoza, Spain.

³Networking Research Center on Bioengineering Biomaterials and Nanomedicine (CIBER-BBN), Madrid, Spain.

⁴Department of Animal Pathology, University of Zaragoza, Zaragoza, Spain

⁵Instituto Universitario de Investigación Mixto Agroalimentario de Aragón (IA2), University of Zaragoza, Zaragoza, Spain.

⁶Instituto Aragonés de Ciencias de la Salud /IIS Aragón, Zaragoza, Spain.

⁷Fundación Araid, Zaragoza, Spain

⁺ Present Address: Department of Molecular Biochemistry and Pharmacology, Instituto di Ricerche Farmacologiche Mario Negri IRCCS, 20156, Milano, Italy.

#Present Address: Department of Surgery, University of Zaragoza Medical School, University of Zaragoza, Zaragoza, Spain.

*Authors for correspondence

KEYWORDS. Extracellular vesicles, optical hyperthermia, gold nanoparticles, multinodular cancer and NIR laser.

Materials and methods

Synthesis and physicochemical characterization of HGNs and PEG-HGNs

All the chemicals employed for the generation of the nanoparticles were purchased from Sigma Aldrich. The synthesis of the HGNs and their functionalization with PEG was performed as described in the bibliography and following previous protocols scaled in our group.^{2,3} Briefly, 400 mL of deionized water, 800 μ L of 0.35 M cobalt chloride hexahydrate and 3.2 mL of 0.1 M sodium citrate were incorporated in a two-neck round-bottom flask and deoxygenated by bubbling argon during 45 min. After that, 4 mL of 1 wt. % PVP and 800 μ L of 1 M sodium borohydride were added to the previous mixture under magnetic stirring during 15 min maintaining the argon bubbling. During this step, cobalt nanoparticles were performed. Then, 380 mL of this nanoparticle dispersion were transferred to a beaker with 120 mL of deionized water mixed with 360 μ L of 0.1 M gold (III) chloride hydrate and was stirred for 30 min to allow the oxidation and the depletion of the sacrificial cobalt nanoparticles and the parallel reduction of the gold on their surface, forming the HGNs. Finally, the particles were washed twice with deionized water by centrifuging them during 12 min at 10000 rpm.

For their functionalization with PEG, the resulted HGNs dispersion was incubated with an excess of monofunctional SH-PEG (Mw=1000 Da) during 30 min with magnetic stirring. Any excess of unbound PEG was eliminated by dialysis against distilled water during 48 h.

As these PEG-HGNs have been widely employed and therefore, thoroughly characterized in our group during last years for the *in vitro* cell culture experiments. Particularly, their cytotoxicity in several cell lines (including, mesenchymal stem cells, fibroblast, HeLa cells and B16-F10) and their capture by these cells have been widely explored by our

group. Because of this detailed previous characterization, only their photothermal properties were assessed in this work. To do that, 1 mL of HGNs (0.12 mg/mL) and PEG-HGNs (0.12 mL) in distilled water or DMEM media were added to a 24 multiwell plate. As control, distilled water and culture media without particles were used. Samples were irradiated during 20 minutes and the temperature was measured with a thermocouple connected to a computer and was registered with the software Laser_2W_4T.

***In vivo* biodistribution evaluation**

In this experiment after 15 days (xenograft model) or 10 days (multinodular model) of tumor implantation, 1.71×10^{10} particles of PEG-HGNs-sEVs^{hpMSCs} (corresponding with 100 μ g expressed in total protein amount) were administered in the tail vein and due to their fluorescence with the Claret probe, their presence in the tumors or in the multicancerous nodules in the pancreas, 24, 48, 72 h and 1 week after administration was visualized under an IVIS equipment. Then, mice were divided in 5 groups according to their day of death: group 1 included control animals which did not receive any treatments; group 2, group 3, group 4 and group 5 received 1.71×10^{10} particles of PEG-HGNs-sEVs^{hpMSCs} (corresponding with 100 μ g expressed in total protein amount) and were sacrificed after 24 h, 48 h, 72 h and 1 week after the intravenous injection, respectively. Animals were euthanized by CO₂ inhalation at the time points indicated before. The **Fig S4** includes an illustration with a summary of the biodistribution study performed in both tumor models.

Tumor, kidneys, liver, lungs, spleen and pancreas were collected from each animal for histopathological analysis (later described) and to evaluate gold bioaccumulation by ICP-MS. To quantify the amount of gold, each organ was digested with Aqua regia (from 1 to 6 mL depending on the volume of the organ) during 5 days at room temperature. Then,

samples were diluted 1/100 in miliQ H₂O and total amount of the metal present within the tissues was determined by ICP-MS (Perkin Elmer Elan DRC-e) in the Chemical Analysis Service from the University of Zaragoza.

Results

Fluorescent stability of PEG-HGNs and PEG-HGNs-sEVs^{hpMSCs}

Once the sEVs were thoroughly characterized, their cell membrane was fluorescently labelled with Claret dye in order to follow and monitor them *in vivo* by IVIS. **Fig S14** shows the stability of the fluorescence labelling in sEVs. To do that, the absorbance at 630 nm was measured in a PEG-HGNs- sEVs^{hpMSCs} solutions stored during 1, 2, 3 and 7 days after their labelling. Moreover, sEVs solutions at these time points were ultracentrifuged and the sEVs pellet was collected and separated from the supernatant to measure the fluorescence in both fractions separately. Those results do not show the appearance of fluorescence in the supernatant during these 7 days, and the levels into the sEVs pellets also kept maintained constant, indicating that the fluorescent dye was not releasing from the sEVs membrane. This data guaranteed that all the fluorescence signal observed *in vivo* is attributed to the sEVs rather than to free released dye.

Tumor model characterization

On the one hand, it is well known that mesenchymal stem cells are able to migrate to damaged and inflammatory areas.¹ On the other hand, it has been recently discovered that sEVs preserve molecular features from their parental cell. Herein, we design two tumor models to explore the possibility of active targeting of these sEVs^{hpMSCs} to enhance the accumulation of the NPs in a xenograft and in a multinodular cancerous model. For the implantation of the primary tumor xenograft model, HeLa cells were employed. They are characterized by their high aggressiveness and fast growth rate. The multinodular model

was generated by the intraperitoneal administration of SKOV3_Luc cells stably infected with a lentivirus expressing the luciferase gene, giving rise to a several and multiple cancerous nodules mainly in the pancreas.

The histopathological H&E analysis allowed us to characterize both tumor models. The xenograft tumors present an expansive and non-encapsulated area with a high neoplastic cell proliferation rate, which was mainly formed by an extensive layer of pleomorphic cells with a polyhedral shape and atypical mitosis. The tumor cells exhibited a spherical or ovoidal shaped nucleus, with a prominent nucleolus and ill-defined eosinophilic areas of the cytoplasm. The stroma of those cells was formed by a scant connective tissue (**Fig S9A**). In the multinodular intraperitoneal model, several cancerous areas were observed attached or integrated in the pancreatic tissue (they were visualized as areas with a high proliferation of neoplastic cells). As in the xenograft models, these SKOV3_Luc tumoral cells presented a spherical or ovoidal shaped nucleus with a marked nucleolus and a non-defined eosinophilic cytoplasm. **Fig S9B** depicts the hematoxylin eosin staining of the pancreas containing the tumor areas. The pancreas shows well defined islets of Langerhans surrounded by exocrine portion of the pancreatic tissue, and by a thin layer of connective tissue. **Fig S9C** includes a conventional IVIS image of one animal with the xenograft subcutaneous model. Finally, the bioluminescence signal of the SKOV3_Luc cells allowed us to image the multinodular tumors in the pancreatic tissue (**Fig S9D**).

Photothermal treatments

The temperatures achieved during the irradiation cycles in mice treated with PEG-HGNs-sEVs^{hpMSCs} or in control mice (untreated) in both tumoral models are shown in **Fig S12**. The results indicate that after 2.5 min of irradiation an increase of 8 and 7,3 °C and only in the animals treated with the sEVs of the xenograft and multinodular model, was observed, respectively. At the end of the irradiation cycle (after 5 min of irradiation), the

temperature reached by the animals treated with the PEG-HGNs-sEVs^{hpMSCs} was 45.8 °C and 41.5 °C in the mice with the xenograft tumor and with the multinodular cancerous areas, respectively. On the contrary, in the control animals of the xenograft and multinodular models, the final temperature achieved was 39.8 °C and 36 °C, respectively.

SUPPLEMENTARY FIGURES

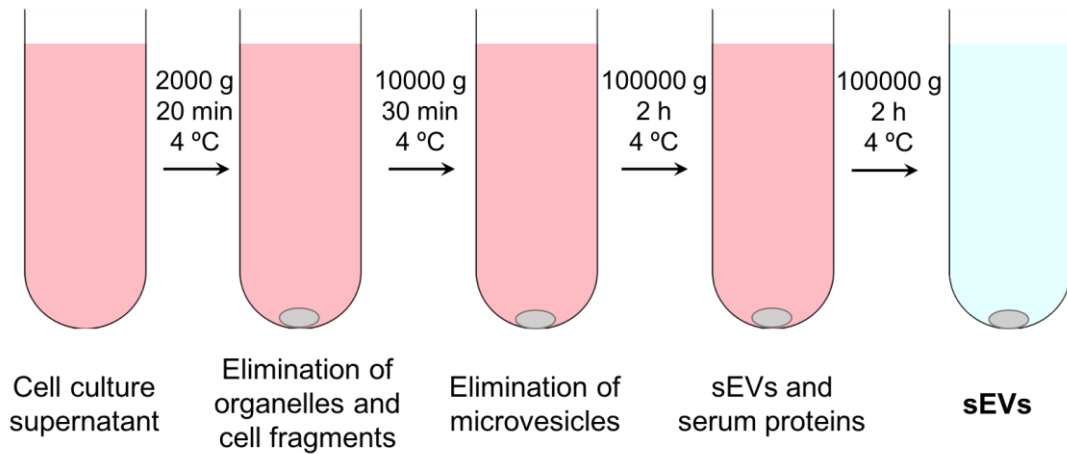


Figure S1. Isolation protocol based on serial ultracentrifugation steps employed for the isolation of sEVs^{hpMSCs} and PEG-HGNs-sEVs^{hpMSCs}.

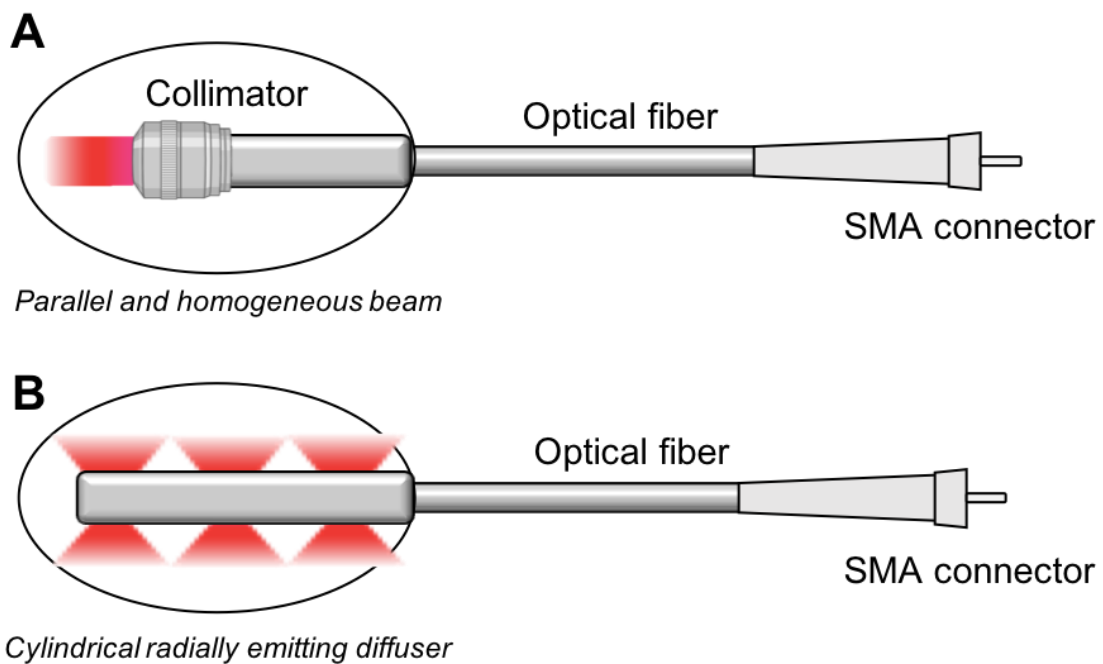


Figure S2. Description of the diffusers employed for: A) Xenograft model (collimator to focus a homogeneous and parallel laser beam in the solid tumor area); and B) Multinodular model (cylindrical radially emitting diffuser to intraperitoneally irradiation of the cancerous nodules localized in the pancreas).

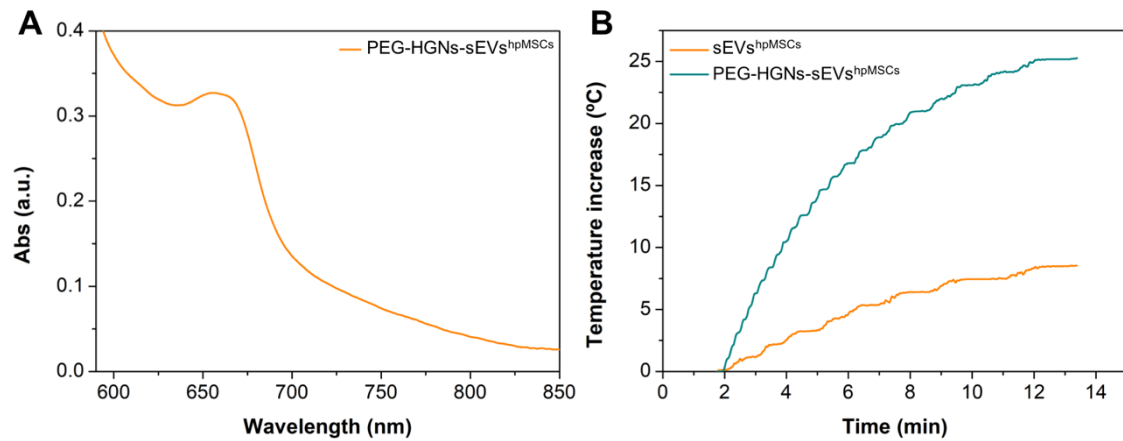


Figure S3. UV-VIS absorption spectra of PEG-HGNs-sEVshpMSCs with a maximum peak in the NIR region. B) Heating efficiency of both sEVshpMSCs and PEG-HGNs-sEVshpMSCs in PBS under NIR light laser irradiation.

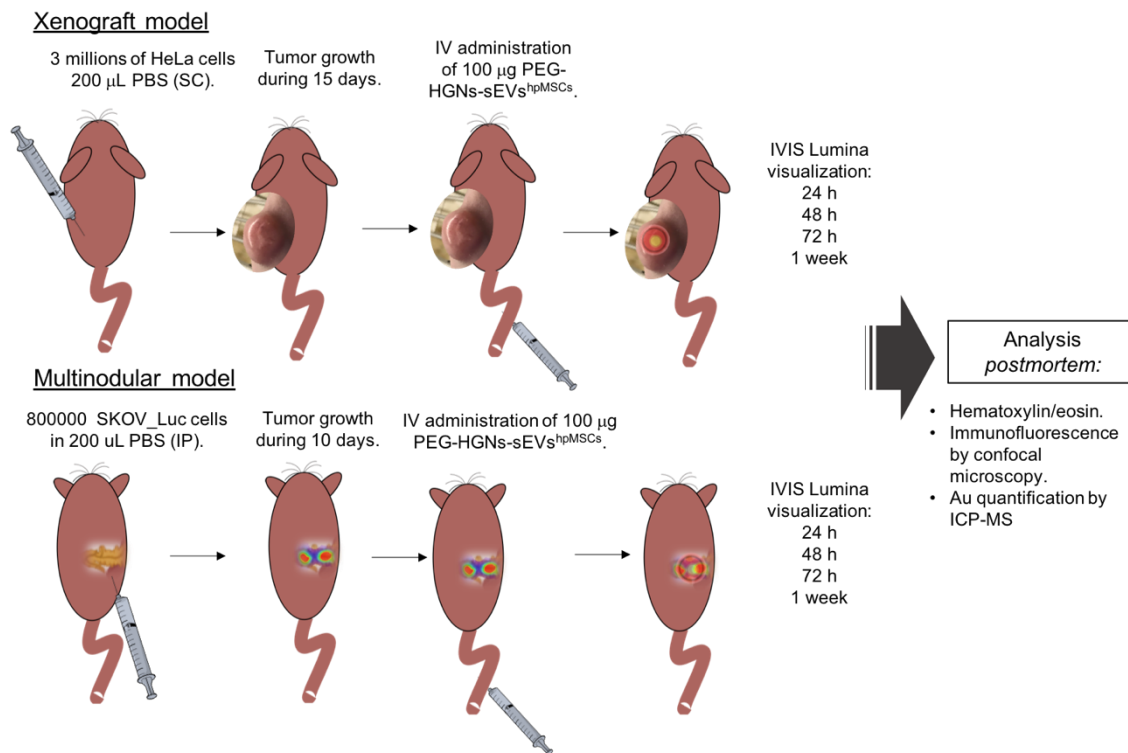


Figure S4. Scheme with the procedure performed for the study of the PEG-HGNs-sEVshpMSCs biodistribution in a xenograft and multinodular tumor models.

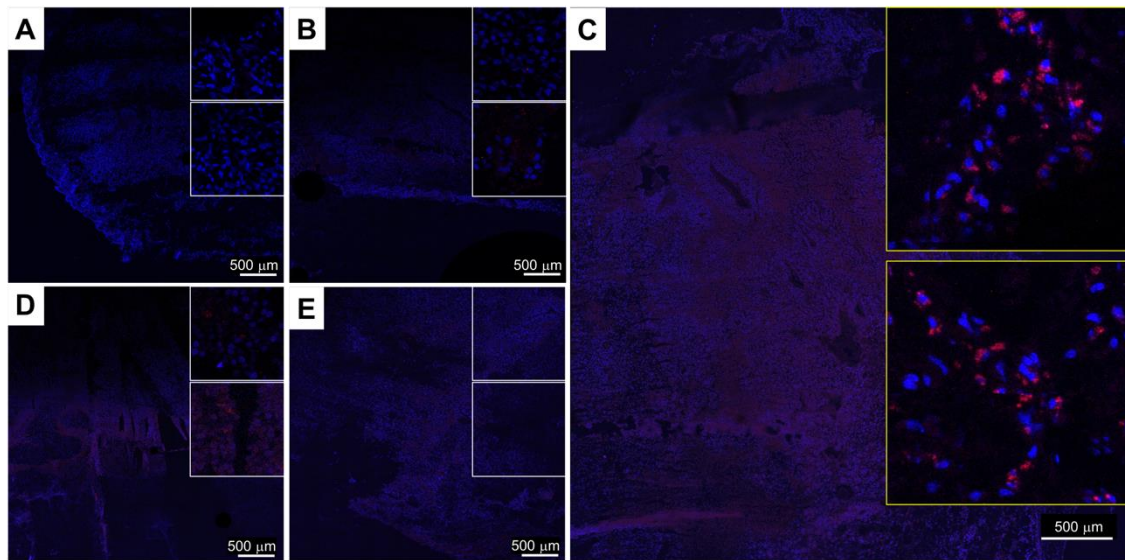


Figure S5. Confocal microscopy images of immunofluorescence labelling of tumor tissues of A) Control (untreated) mice; or mice treated with PEG-HGNs-sEVs^{hpMSCs} and sacrificed after B) 1; C) 2, D) 3 and E) 7 days.

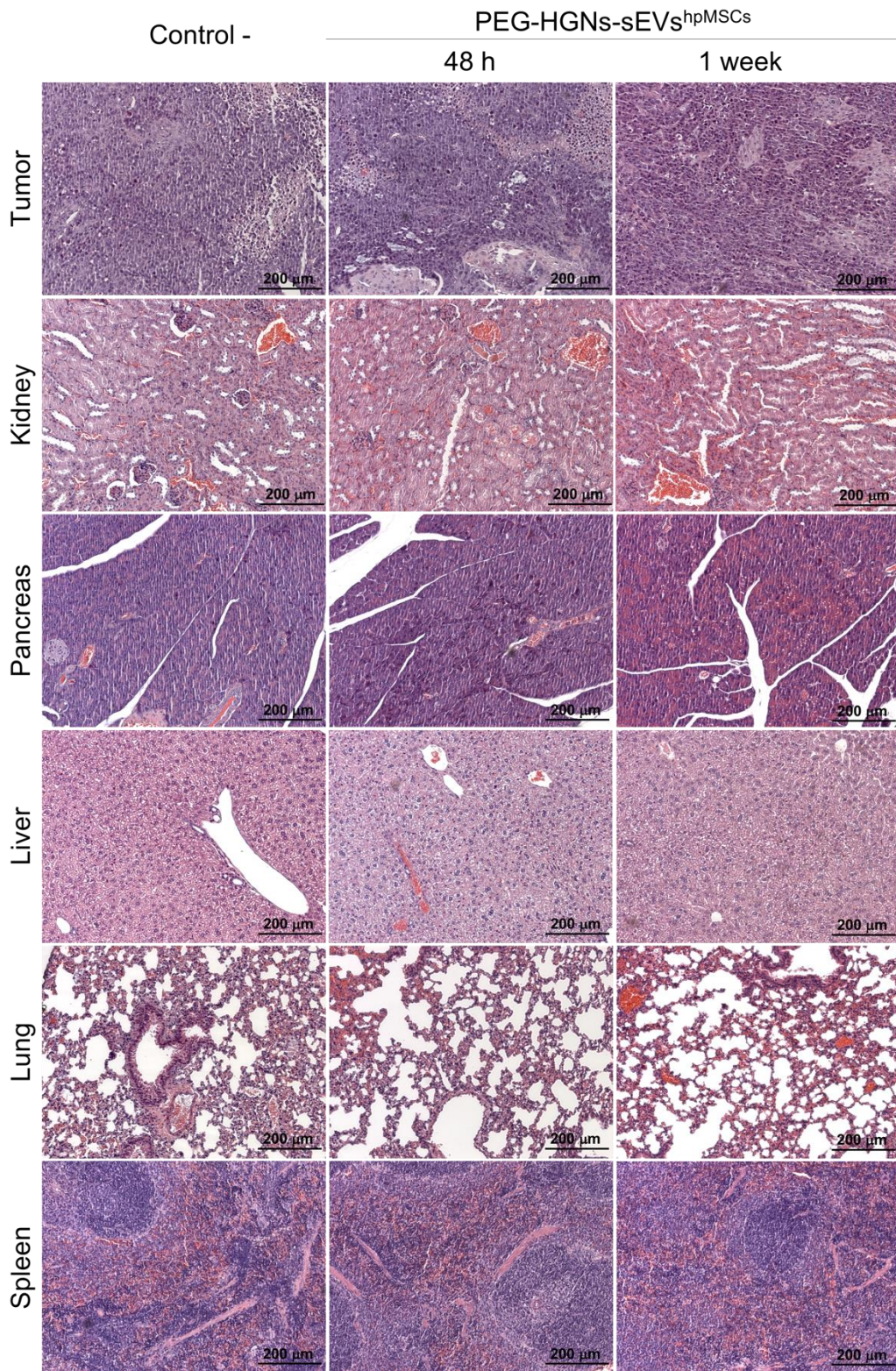


Figure S6. Hematoxylin and eosin tissue sections from control (untreated) and PEG-HGNs-sEVs^{hpMSCs} treated mice at 48 h and 1 week after intravenous sEVs administration. The tumor and the studied organs of treated mice did not show significant histopathologic changes that could be attributed to the presence of sEVs, when compared to controls.

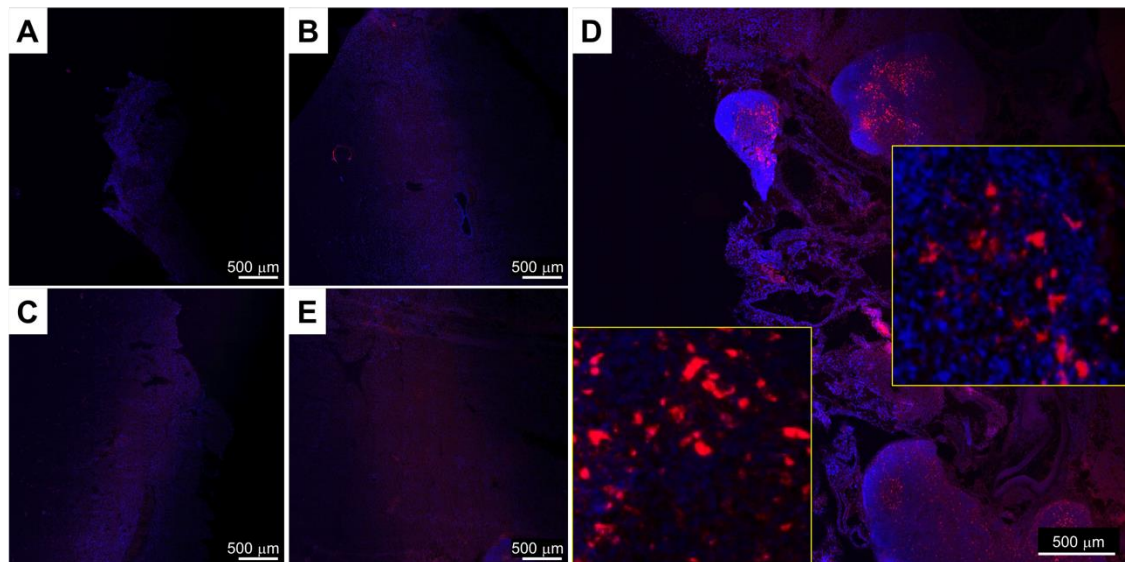


Figure S7. Confocal microscopy images of immunofluorescence labelling of pancreatic tissue in mice with the multinodular model: A) Control (untreated) mice; or mice treated with PEG-HGNs-sEVs^{hpMSCs} and sacrificed after B) 24 h; C) 48 h, D) 72 h and E) 1 week.

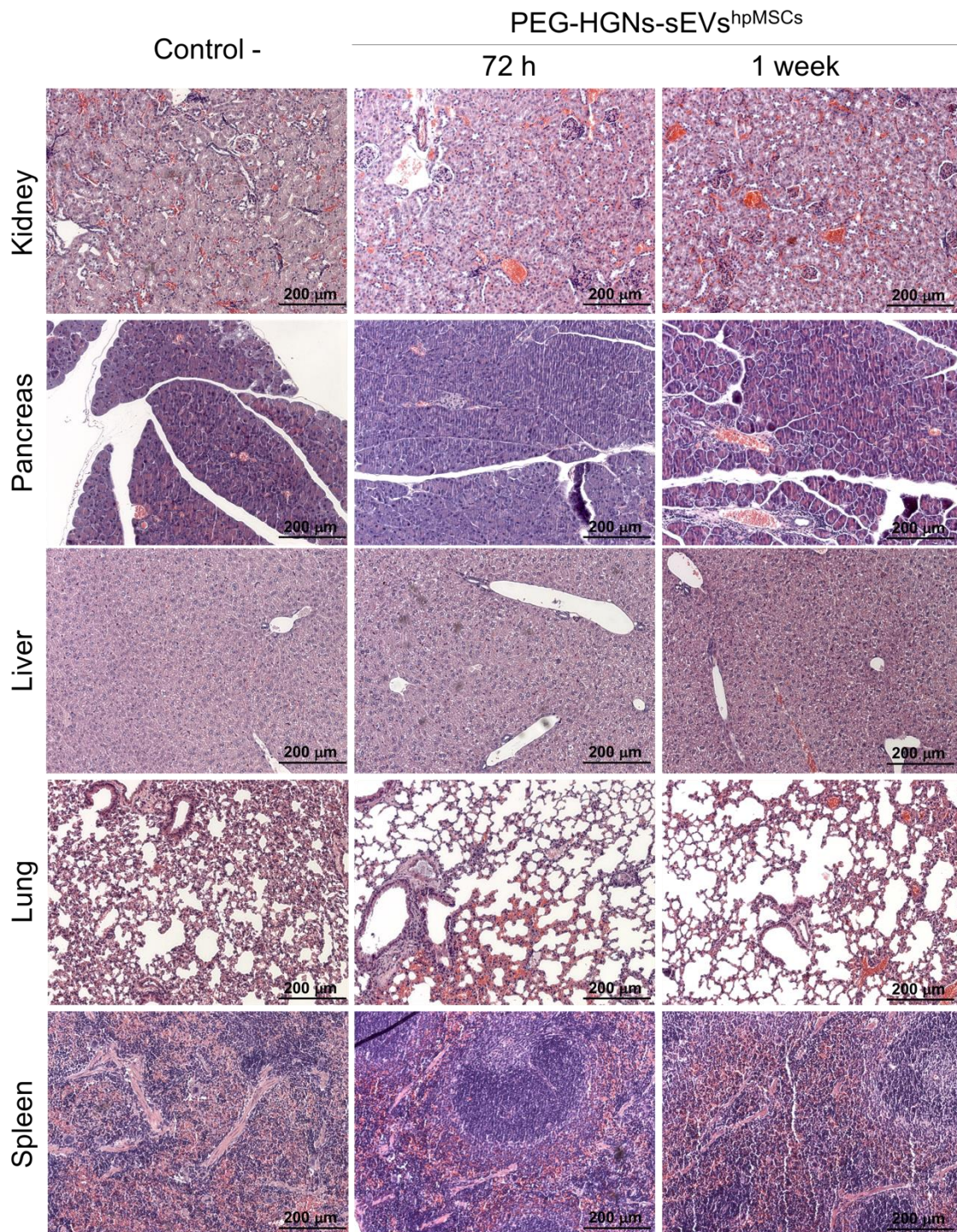


Figure S8. Hematoxylin and eosin tissue sections from control (untreated) and PEG-HGNs-sEVs^{hpMSCs} treated mice (both with multinodular tumors implanted) at 72 h and 1 week after intravenous sEVs administration. The tumor and organs studied in treated mice did not show significant histopathologic changes that could be attributed to the presence of sEVs, when compared to controls.

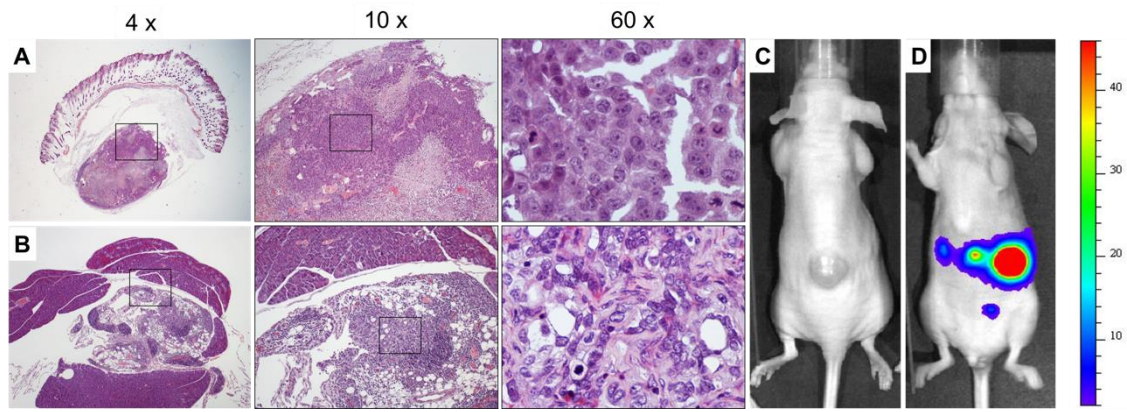


Figure S9. A) Hematoxylin-eosin staining resulted for histological sections of xenograft tumor. B) Hematoxylin-eosin staining analysis of the multinodular model of a pancreas with cancerous areas. Highly cellular pleomorphic neoplastic proliferation cells were observed. C) IVIS image of an animal with the xenograft model implanted. D) IVIS image of an animal with the multinodular tumor model.

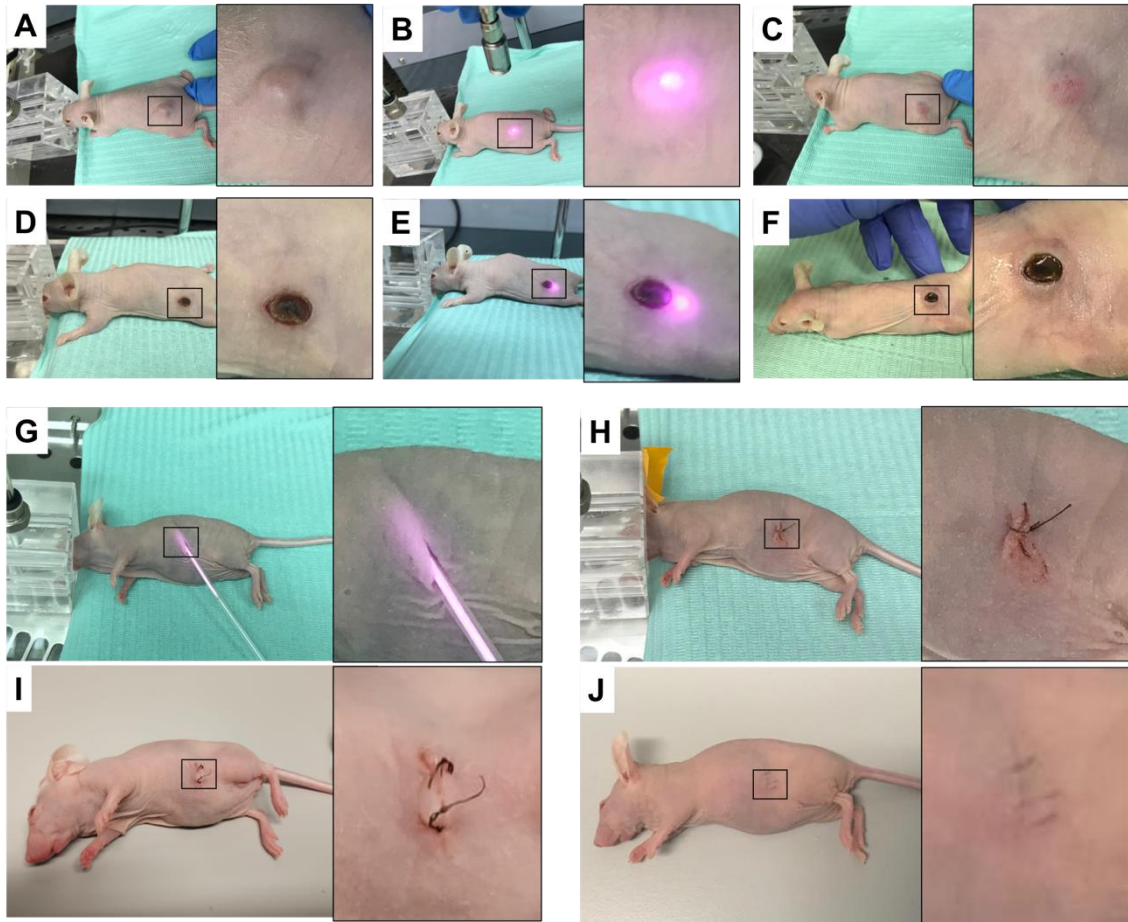


Figure S10. Experimental sequence of the irradiation procedure performed in both tumor models (in the xenograft tumor: A-F; and in the multinodular: G-J).

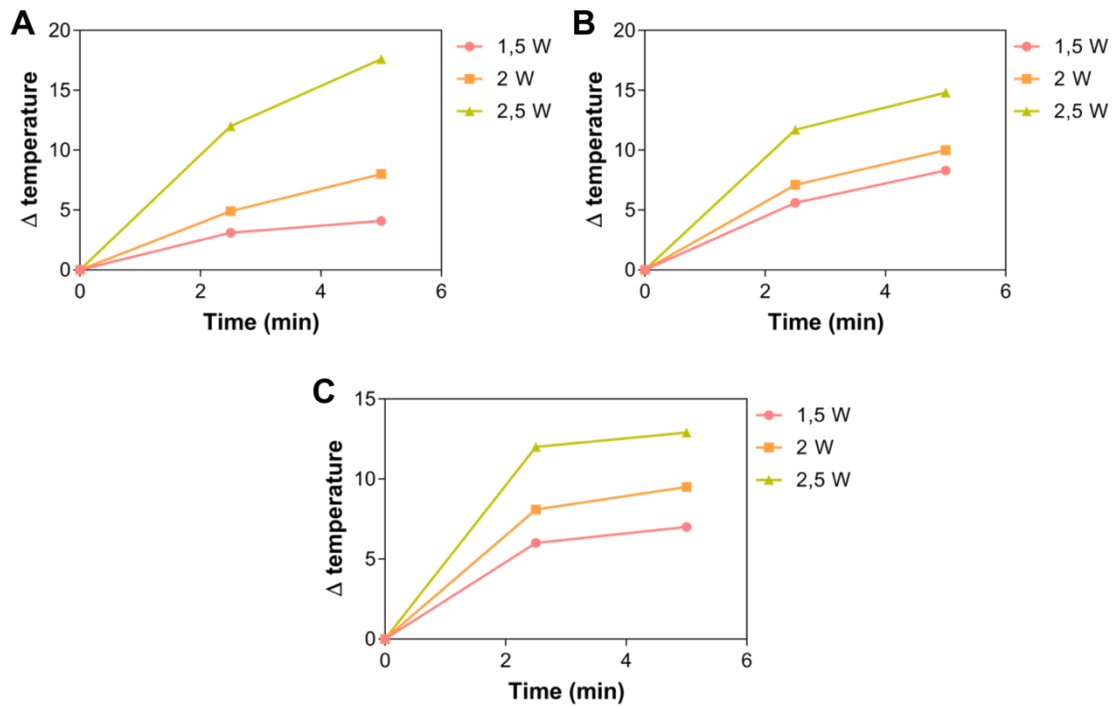


Figure S11. *Ex vivo* irradiation of different organs containing PEG-HGNs with different laser powers. A) Liver, B) spleen and C) pancreas.

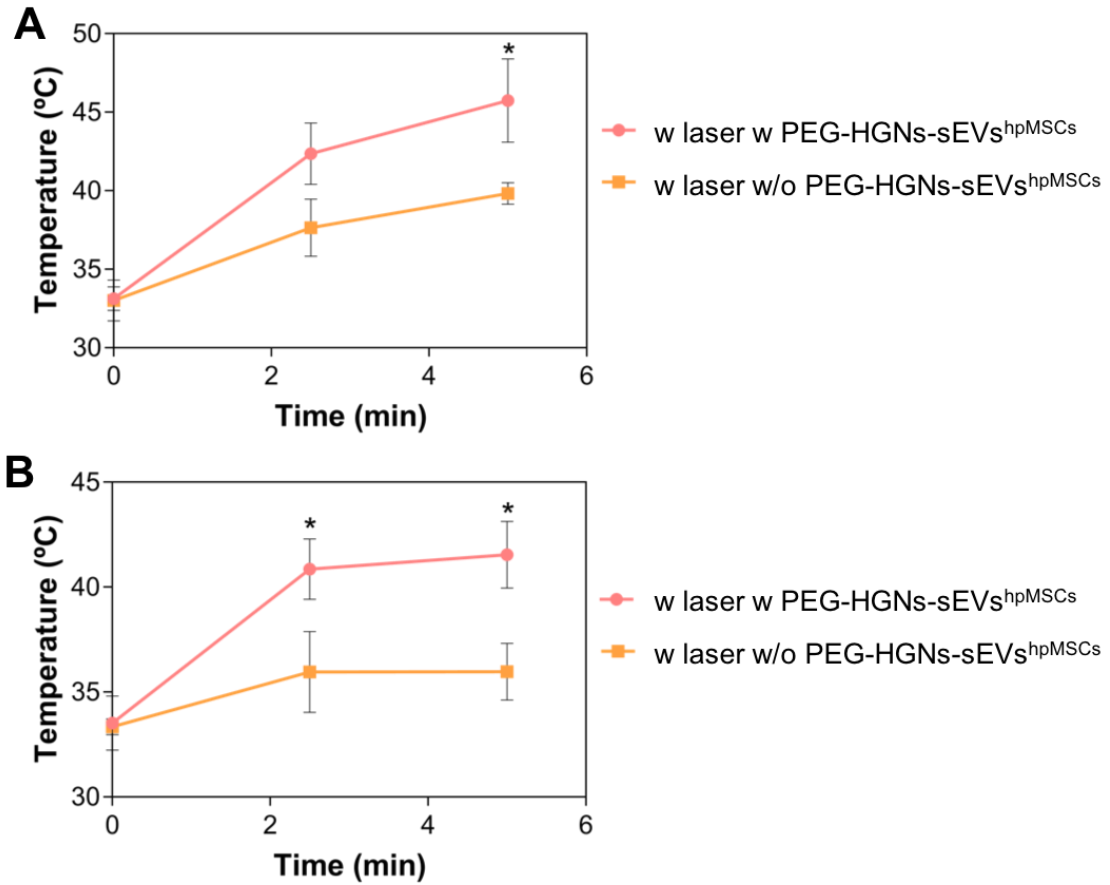


Figure S12. The temperatures achieved during the irradiation cycles in mice treated with PEG-HGNs-sEVs^{hpMSCs} or in control mice (untreated) in A) xenograft and B) multinodular models. *p<0.05.

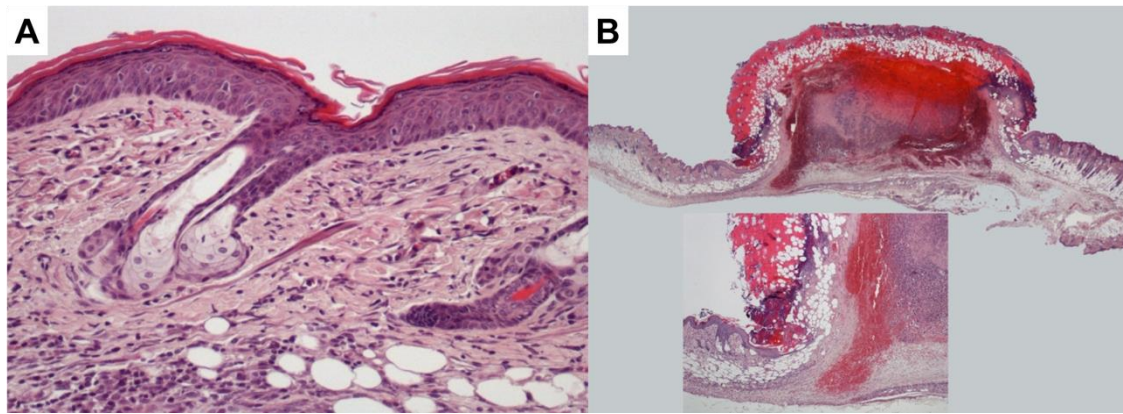


Figure S13. A) Skin from mouse treated with laser, without sEVs. Intact epidermis and dermis over the tumor mass. HE, 20x original power. B) Skin and tumor mass from mice treated with sEVs and laser. The skin above the tumor and the tumor itself are coagulated as a result of overheating. Normal skin is observed at both sides of the tumor mass. HE, 1x original power. Inset: Detail of the junction between normal skin and overheated tissue. HE, 4x original power.

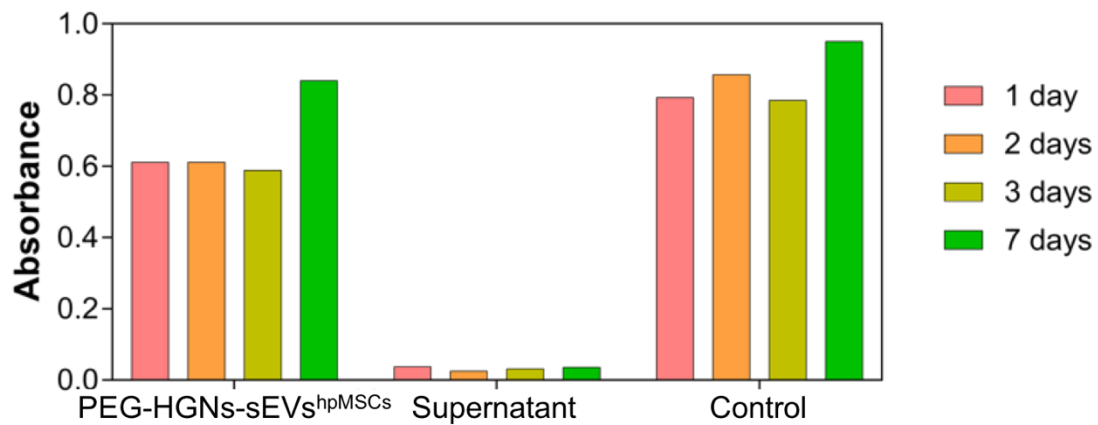


Figure S14. Stability of sEVs fluorescently labeled during 1, 2, 3, and 7 days after their labelling.

References

1. Belmar-Lopez, C. *u.c.* Tissue-derived mesenchymal stromal cells used as vehicles for anti-tumor therapy exert different in vivo effects on migration capacity and tumor growth. *BMC Med.* **11**, 139 (2013).
2. Preciado-flores, S., Wang, D., Wheeler, D. A., Newhouse, R. & Hensel, J. K. Highly reproducible synthesis of hollow gold nanospheres with near infrared surface plasmon absorption using PVP as stabilizing agent. *J. Mater. Chem.* **21**, 2344–2350 (2011).
3. Sancho-Albero, M., Navascués, N., Mendoza, G., Sebastián, V. & Arruebo, M. Exosome origin determines cell targeting and the transfer of therapeutic nanoparticles towards target cells. *J. Nanobiotechnology* **17**, 1–13 (2019).
4. Sancho-albero, M., Navascués, N., Mendoza, G., Sebastián, V. & Arruebo, M. Exosome origin determines cell targeting and the transfer of therapeutic nanoparticles towards target cells. *J. Nanobiotechnology* **17**, 1–13 (2019).